



Assembly of Lanthanide-Containing Tungstotellurates(VI): Syntheses, Structures, and Catalytic Properties

Jie Li¹, Shuxia Shang², Zhengguo Lin¹, Zishuo Yao¹, Ni Zhen¹, Zhen Li¹, Yingnan Chi^{1*} and Changwen Hu^{1*}

¹ Key Laboratory of Cluster Science Ministry of Education, Beijing Key Laboratory of Photoelectronic/Electrophotonic Conversion Materials, School of Chemistry and Chemical Engineering, Beijing Institute of Technology, Beijing, China, ² China Resources Double-Crane Pharmaceutical Co., Ltd., Beijing, China

OPEN ACCESS

Edited by:

Jingyang Niu,
Henan University, China

Reviewed by:

Zhi-Ming Zhang,
Tianjin University of Technology, China
Helene Serier-Brault,
UMR6502 Institut des Matériaux Jean
Rouxel (IMN), France

*Correspondence:

Yingnan Chi
chiyingnan7887@bit.edu.cn
Changwen Hu
cwhu@bit.edu.cn

Specialty section:

This article was submitted to
Inorganic Chemistry,
a section of the journal
Frontiers in Chemistry

Received: 26 August 2020

Accepted: 05 October 2020

Published: 23 November 2020

Citation:

Li J, Shang S, Lin Z, Yao Z, Zhen N,
Li Z, Chi Y and Hu C (2020) Assembly
of Lanthanide-Containing
Tungstotellurates(VI): Syntheses,
Structures, and Catalytic Properties.
Front. Chem. 8:598961.
doi: 10.3389/fchem.2020.598961

Lanthanide (Ln)-containing polyoxometalates (POMs) have attracted particular attention owing to their structural diversity and potential applications in luminescence, magnetism, and catalysis. Herein three types of Ln-containing tungstotellurates(VI) (Ln = Dy³⁺, Ho³⁺, Er³⁺, Tm³⁺, Yb³⁺, and Lu³⁺), dimeric (DMAH)_n[H_{22-n}{Ln(H₂O)₃[TeW₁₇O₆₁]}₂]·mH₂O (abbreviated as {Ln₂Te₂W₃₄}; DMAH⁺ = dimethylammonium), mono-substituted (DMAH)₇Na₂{H₂Ln(H₂O)₄[TeW₁₇O₆₁]}·mH₂O (abbreviated as {LnTeW₁₇}), and three-dimensional (3D) inorganic frameworks (DMAH)_n{H_{3-n}Ln(H₂O)₄[TeW₆O₂₄]}·mH₂O (abbreviated as {LnTeW₆}), have been synthesized by using simple metal salts and characterized by single-crystal X-ray diffraction and other routine techniques. Interestingly, the assembly of these POMs is pH dependent. Using the same starting materials, {Ln₂Te₂W₃₄} were obtained at pH 1.7, where two Dawson-like monovacant [TeW₁₇O₆₁]¹⁴⁻ are linked by two Ln³⁺ ions; mono-substituted Dawson-like {LnTeW₁₇} were isolated at pH 1.9, and 3D inorganic framework {LnTeW₆} based on Anderson-type [TeW₆O₂₄]⁶⁻ were formed at pH 2.3. It was also found that the assembly of Ln-containing POMs depends on the type of Ln³⁺ ions. The three types of POMs can be prepared by using Ln³⁺ ions with a relatively smaller ionic radius, such as Tb³⁺-Lu³⁺, while the use of Ln³⁺ ions (La³⁺-Eu³⁺) results in the formation of precipitation or {TeW₁₈O₆₂} clusters. Furthermore, three {LnTeW₆} (Ln = Tb³⁺, Er³⁺, Lu³⁺) were used as Lewis acid catalysts for the cyanosilylation of benzaldehydes, and their catalytic activity decreases with the decrease of Ln³⁺ ionic radius, giving the order: {TbTeW₆} > {ErTeW₆} > {LuTeW₆}. Notably, {TbTeW₆} is stable to leaching and can be reused for five cycles without a significant loss of its activity.

Keywords: polyoxometalates, tungstotellurates(VI), lanthanide ions, self-assembly, Lewis acidic catalysis, cyanosilylation

INTRODUCTION

Polyoxometalates (POMs) are a unique class of metal-oxo clusters with tunable structures and excellent properties (Hill, 1998; Cronin and Müller, 2012). Due to the existence of abundant surface oxygen atoms, POMs as inorganic ligands can easily coordinate with transition metal or lanthanide (Ln) ions, resulting in the formation of discrete nanoscale clusters or extended

structures. Among them, Ln-containing polyoxotungstates have attracted numerous attention owing to their structural diversity (Ma et al., 2015; Zhao et al., 2016b) and attractive applications in luminescence (Granadeiro et al., 2010; Ritchie et al., 2010b), magnetism (Clemente-Juan et al., 2012; Suzuki et al., 2013), and catalysis (Boglio et al., 2006; Suzuki et al., 2014; Li et al., 2018). Up to now, two synthetic strategies have been developed to construct Ln-containing POMs. One is building block method, where different lacunary POM precursors, such as monolacunary $[XW_{11}O_{39}]^{n-}$ (Zhang et al., 2012; Arab Fashapoyeh et al., 2018; Mougharbel et al., 2020) and trilacunary $[XW_9O_{34}]^{n-}$ ($X = P, Si, Ge$) (Zhao et al., 2014, 2017) and $[XW_9O_{33}]^{9-}$ ($X = As^{III}, Sb^{III}$) (Chen et al., 2018; Kaushik et al., 2018), were used to coordinate with Ln^{3+} ions. The other is one-pot synthetic strategy, by which intricate POM structures are fabricated through the condensation reaction of simple metal salts with heteroanions (Chen et al., 2013, 2014; Zhao et al., 2016a; Liu J. C. et al., 2018). Although the one-pot method is simple and straightforward, understanding the assembly process is challenging.

Generally, the assembly of Ln-containing POMs can be affected by many synthetic parameters, such as molar ratio of reactants, temperature, pH, solvents, and so on. Among them, the pH value is a key factor. For example, Chen et al. reported five Ce(III)-containing POMs, finding that the structural motif of POM building block can be influenced by the pH value (Chen et al., 2014). Subsequently, they also demonstrated that pH can control the arrangement of lacunary Keggin and Wells–Dawson clusters (Chen et al., 2019). Moreover, the type of Ln^{3+} ions plays a role during the formation of Ln-containing POMs. Ozeki and Yamase reported the effect of lanthanide contraction on the Ln–O bond lengths in $[LnW_{10}O_{36}]^{10-}$ clusters ($Ln = Pr, Nd, Sm, Gd, Tb, Dy$) (Ozeki and Yamase, 1994). Previous investigations indicate that the arrangement of POM can also be influenced by the type of Ln^{3+} ions. For example, the assembly of monovacant $[\alpha-SiW_{11}O_{39}]^{8-}$ with different Ln^{3+} ions leads to three different structural motifs: 1D linear chain $[Yb(\alpha-SiW_{11}O_{39})(H_2O)_2]^{5-}$, 1D zigzag chain $[Eu(\alpha-SiW_{11}O_{39})(H_2O)_2]^{5-}$, and 2D network $[Nd_2(\alpha-SiW_{11}O_{39})(H_2O)_{11}]^{2-}$ (Mialane et al., 2003). In 2007, Kortz et al. found that the configuration of POMs can change with the size of Ln^{3+} ions. For example, $[Ln(\beta_2-GeW_{11}O_{39})_2]^{13-}$ was isolated when using a larger Ln^{3+} ion ($Ln = La, Ce, Pr, Nd, Sm, Gd, or Dy$), while $[Ln(\beta_2-GeW_{11}O_{39})]^{13-}$ was prepared when using a smaller Ln^{3+} ion ($Ln = Ho, Er, or Tm$) (Mougharbel et al., 2020).

Tungstotellurates are an important subfamily of polyoxotungstates with trigonal–pyramidal $\{Te^{IV}O_3\}^{2-}$ or octahedral $\{Te^{VI}O_6\}^{6-}$ as heteroanions. Due to the existence of lone pair electrons in Te(IV) atom, tungstotellurates(IV) tend to form lacunary structures, such as $[H_2Te_4W_{20}O_{80}]^{22-}$ and $[NaTeW_{15}O_{54}]^{13-}$ (Ismail et al., 2009), dimeric $[Te_2W_{17}O_{61}]^{12-}$, $[Te_2W_{16}O_{58}(OH)_2]^{14-}$, and $[Te_2W_{18}O_{62}(OH)_2]^{10-}$ (Ritchie et al., 2010a), as well as macrocyclic clusters: $[W_{28}Te_8O_{112}]^{24-}$, $[W_{28}Te_9O_{115}]^{26-}$, and $[W_{28}Te_{10}O_{118}]^{28-}$ (Gao et al., 2011). Therefore, Ln^{3+} ions can be readily incorporated into tungstotellurates(IV) (Chen et al., 2013, 2015; Han et al., 2017a,b; Liu J. L. et al., 2018; Liu et al., 2019; Zhang et al., 2020). In comparison, limited attention

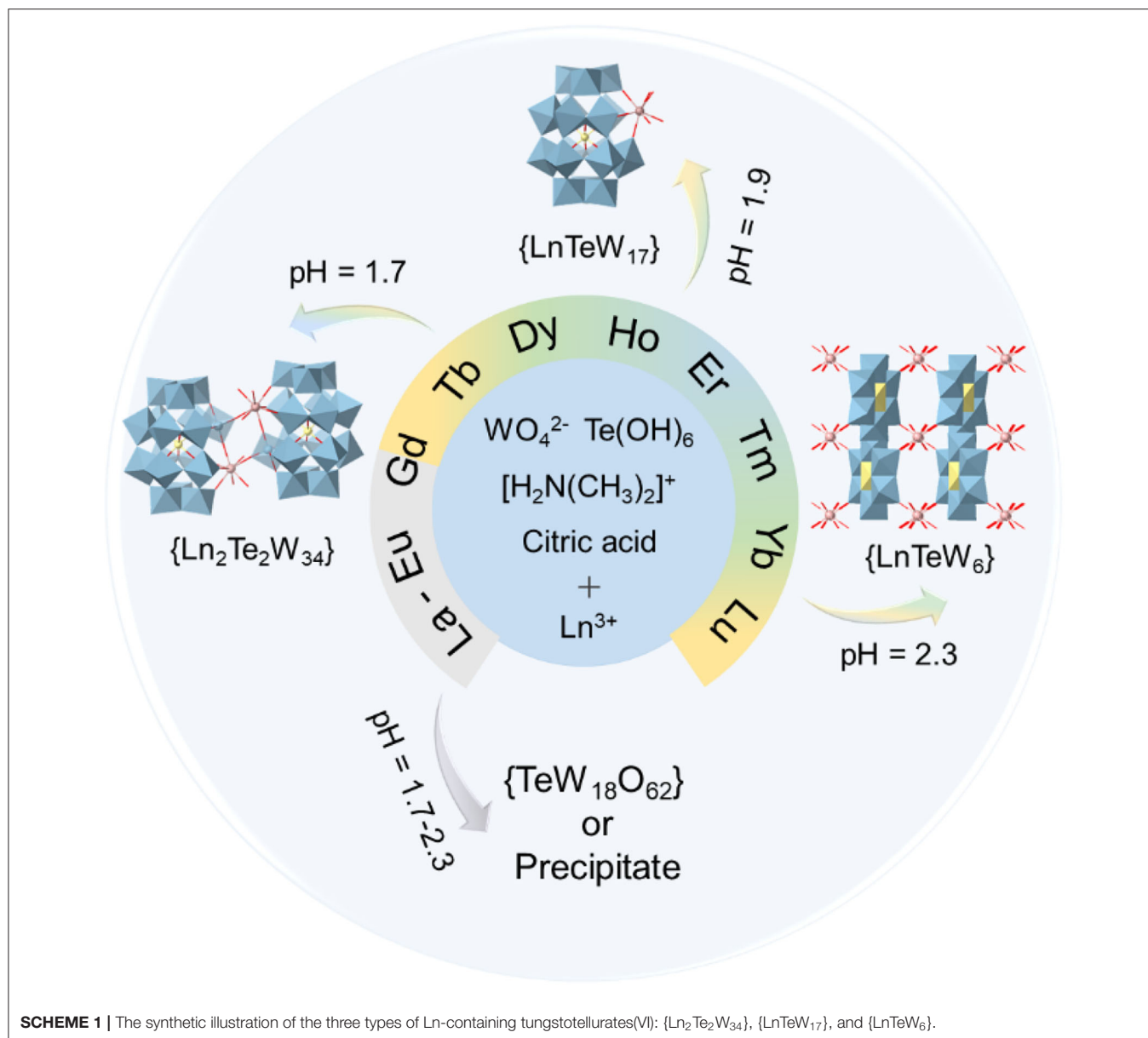
has been paid on tungstotellurates(VI). The first member of tungstotellurates(VI) is Anderson-type $[TeW_6O_{24}]^{6-}$, which was first determined in 1986 (Schmidt et al., 1986). After that, until 2009 two new members, Dawson-like $[H_3W_{18}O_{56}(Te^{VI}O_6)]^{7-}$ ($\{TeW_{18}O_{62}\}$) and high nuclearity $[H_{10}Te_2^{VI}W_{58}O_{198}]^{26-}$, were discovered by Cronin and Long (Yan et al., 2009). As the reported tungstotellurates(VI) are plenary clusters, Ln-containing tungstotellurates(VI) was nearly unexplored. Recently, Ln^{3+} ions ($Ln = Eu, Gd, Tb$) have been successfully introduced into tungstotellurates(VI) in our group, obtaining dimeric $[H_{10}(WO_2)\{Ln(H_2O)_5(Te^{VI}W_{18}O_{65})_2\}]^{12-}$ ($Ln = Eu, Gd, Tb$) and tetrameric $[H_{16}\{Ln(H_2O)_5(Te^{VI}W_{18}O_{64})_4\}]^{28-}$ ($Ln = Eu, Gd$), dimeric $[H_6\{Tb(H_2O)_3(Te^{VI}W_{17}O_{61})_2\}]^{12-}$, mono-substituted $[H_2Tb(H_2O)_4(Te^{VI}W_{17}O_{61})]^{9-}$, and 3D inorganic framework $[HTb(H_2O)_4\{Te^{VI}W_6O_{24}\}]^{2-}$ (Shang et al., 2018). In the synthetic process, we find that the assembly of Tb-containing tungstotellurates(VI) is controlled by pH and that the formation of tetrameric clusters depends on the type of Ln^{3+} ions.

To systematically investigate the effect of Ln^{3+} ions on the assembly of Ln-containing tungstotellurates(VI), herein the Ln source was extended from La^{3+} to Lu^{3+} (except radioactive Pm^{3+}). When Ln^{3+} ($Tb^{3+}, Dy^{3+}, Ho^{3+}, Er^{3+}, Tm^{3+}, Yb^{3+}, Lu^{3+}$) with a relatively smaller ionic radius was used in the assembly, dimeric $(DMAH)_n[H_{22-n}\{Ln(H_2O)_3[TeW_{17}O_{61}]\}_2] \cdot mH_2O$ (abbreviated as $\{Ln_2Te_2W_{34}\}$, $DMAH^+$ = dimethylammonium), mono-substituted $(DMAH)_7Na_2\{H_2Ln(H_2O)_4[TeW_{17}O_{61}]\} \cdot mH_2O$ (abbreviated as $\{LnTeW_{17}\}$), and 3D inorganic frameworks $(DMAH)_n\{H_{3-n}Ln(H_2O)_4[TeW_6O_{24}]\} \cdot mH_2O$ (abbreviated as $\{LnTeW_6\}$) were formed at pH 1.7, 1.9, and 2.3, respectively. However, under the otherwise identical conditions, no crystal compounds were generated by using La^{3+} – Eu^{3+} with a relatively larger ionic radius (**Scheme 1**). The three types of Ln-containing tungstotellurates(VI) have been characterized by single-crystal X-ray diffraction, Fourier-transform infrared (FT-IR) spectra, elemental analyses, and TG analyses. Moreover, $\{LnTeW_6\}$ ($Ln = Tb^{3+}, Er^{3+}, Lu^{3+}$) were used as Lewis acid catalysts to catalyze the cyanosilylation of aldehydes or ketone with trimethylsilylcyanide (TMSCN) under solvent-free conditions, and the relationship between the radii of Ln^{3+} ions and catalytic activity was also investigated.

EXPERIMENTAL

Materials

Most of the chemicals were purchased from the following manufacturers: Aladdin ($PrCl_3$, 99.9%; $TbCl_3 \cdot 6H_2O$, 99.9%; $HoCl_3 \cdot 6H_2O$, 99.9%; $LuCl_3 \cdot 6H_2O$, 99.9%; citric acid monohydrate, 99.5%; trimethylsilylcyanide, 96%), Energy chemical ($[NdCl_3 \cdot 6H_2O]$, 99.99%; $[SmCl_3 \cdot 6H_2O]$, 99.99%; $[EuCl_3 \cdot 6H_2O]$, 99.99%; $[GdCl_3 \cdot 6H_2O]$, 99.99%; $[DyCl_3 \cdot 6H_2O]$, 99.99%; $[ErCl_3 \cdot 6H_2O]$, 99.99%; $[TmCl_3 \cdot 6H_2O]$, 99.99%; dimethylamine hydrochloride, 98%; α -(trimethylsilyloxy)phenylacetone nitrile, 97%), Alfa Aesar ($[YbCl_3 \cdot 6H_2O]$, 99.9%), and Sinopharm Chemical Reagent



Co., Ltd. ($\text{Na}_2\text{WO}_4 \cdot 2\text{H}_2\text{O}$, AR; $\text{LaCl}_3 \cdot n\text{H}_2\text{O}$, AR; $\text{CeCl}_3 \cdot 6\text{H}_2\text{O}$, 99%; benzaldehyde, AR; acetophenone, AR). These reagents were used without further purification, except benzaldehyde. The Anderson-type tungstotellurates(VI), $\text{Na}_6\text{TeW}_6\text{O}_{24} \cdot 22\text{H}_2\text{O}$, was prepared according to the literature (Shah et al., 2014).

Characterizations

FT-IR spectra were recorded on a Thermo IS5 spectrophotometer in the $4,000\text{--}400\text{ cm}^{-1}$ region as KBr-pressed pellets. Thermogravimetric analyses were carried out under flowing N_2 on a Shimadzu DTG-60H instrument at a heating rate of $10^\circ\text{C}/\text{min}$. Elemental analyses (C, H, and N) were performed on ELEMENTAR vario EL cube Elmer CHN elemental analyzer. The Ln, W, Na, and Te elements were measured with ThermoCAP Q mass spectrometry. The morphologies of $\{\text{TbTeW}_6\}$ were

observed on a JEOL model S-4800 field-emission scanning electron microscopy with an accelerating voltage of 5 kV. The catalytic reaction was monitored on a Shimadzu GC-2014C instrument with a flame ionization detector.

X-ray Crystallography

The X-ray single crystal diffraction data were collected on a Bruker APEX-II CCD diffractometer with graphite monochromatic Mo-K α radiation ($\lambda = 0.71073\text{ \AA}$) at 296 K. All crystals were sealed in capillary glass tubes for testing. All structures were solved using an intrinsic phasing method (SHELXT) (Sheldrick, 2015) and refined by full-matrix least-squares against F_o^2 with SHELXL software package (Sheldrick, 2015). Moreover, the residual disordered or crystal solvent molecules and cations were estimated by using the solvent

MASK routine of OLEX2 (similar to PLATON/SQUEEZE) (Dolomanov et al., 2009). The hydrogen atoms were not incorporated in the refinements, and all non-hydrogen (Ln, W, Te, C, N, and O) atoms were refined anisotropically. The lattice H₂O molecules and cations can be partly found from the Fourier maps, but not all lattice H₂O molecules and cations can be found from the weak residual electron peaks. Thus, the numbers of the cations and lattice H₂O molecules were determined and added to the molecular formula directly on the basis of elemental analyses, TG analyses, and the charge balance consideration. The crystallographic data for these crystal compounds are summarized in **Supplementary Table 1**. The crystallographic data have been deposited with the Cambridge Crystallographic Data Center with CCDC 2023272-2023277 for {Ln₂Te₂W₃₄}, 2023278-2023283 for {LnTeW₁₇}, and 2023284-2023289 for {LnTeW₆} (Ln = Dy³⁺, Ho³⁺, Er³⁺, Tm³⁺, Yb³⁺, and Lu³⁺), respectively.

Synthesis of (DMAH)_n[H_{22-n}{Ln(H₂O)₃[TeW₁₇O₆₁]}₂]⁻ mH₂O: ({Ln₂Te₂W₃₄}, Ln = Dy³⁺, *n* = 16, *m* = 23; Ho³⁺, *n* = 15, *m* = 24; Er³⁺, *n* = 15, *m* = 25; Tm³⁺ and Yb³⁺, *n* = 15, *m* = 28; Lu³⁺, *n* = 15, *m* = 30).

A mixture containing Na₂WO₄·2H₂O (4.50 mmol, 1.50 g), Te(OH)₆ (0.44 mmol, 0.10 g), dimethylamine hydrochloride (7.35 mmol, 0.60 g), citric acid monohydrate (0.26 mmol, 0.05 g), and distilled water (20 mL) was charged to a 25 ml glass beaker. The pH was adjusted to 4.5 by dropping 6 M HCl under stirring. After that, LnCl₃·6H₂O (0.33 mmol, 0.12 g) was added to the mixture, forming a uniform suspension and the pH was adjusted to 1.7. The suspension was stirred at room temperature for about 5 min and filtered. The clear filtrate was placed in a refrigerator at 10°C for 5 days and then evaporated at the ambient environment after filtering again. The cubic-shaped crystals were observed after 1 month, and at that time, the pH of the mother liquor is 2.7. Element analysis (%) for {Dy₂Te₂W₃₄}: calcd. C 3.83, N 2.23, W 62.2, Te 2.54, Dy 3.23; found: C 3.39, N 2.06, W 61.2, Te 2.53, Dy 3.12; yield: 34% based on W. Element analysis (%) for {Ho₂Te₂W₃₄}: calcd. C 3.59, N 2.10, W 62.3, Te 2.55, Ho 3.29; found: C 3.41, N 2.10, W 61.3, Te 2.57, Ho 3.15; yield: 30% based on W. Element analysis (%) for {Er₂Te₂W₃₄}: calcd. C 3.59, N 2.09, W 62.2, Te 2.54, Er 3.33; found: C 3.70, N 2.29, W 60.5, Te 2.60, Er 3.10; yield: 32% based on W. Element analysis (%) for {Tm₂Te₂W₃₄}: calcd. C 3.57, N 2.08, W 61.8, Te 2.53, Tm 3.34; found: C 3.61, N 2.24, W 62.0, Te 2.60, Tm 3.30; yield: 35% based on W. Element analysis (%) for {Yb₂Te₂W₃₄}: calcd. C 3.56, N 2.08, W 61.8, Te 2.52, Yb 3.42; found: C 3.57, N 2.11, W 61.2, Te 2.50, Yb 3.23; yield: 36% based on W. Element analysis (%) for {Lu₂Te₂W₃₄}: calcd. C 3.55, N 2.07, W 61.6, Te 2.51, Lu 3.45; found: C 3.61, N 2.14, W 61.3, Te 2.60, Lu 3.40; yield: 37% based on W.

Synthesis of (DMAH)₇Na₂{H₂Ln(H₂O)₄[TeW₁₇O₆₁]}⁻ mH₂O: ({LnTeW₁₇}, Ln = Dy³⁺, *m* = 23; Ho³⁺ and Lu³⁺, *m* = 27; Er³⁺, *m* = 22; Tm³⁺, *m* = 21; Yb³⁺, *m* = 26).

The synthetic procedure of {LnTeW₁₇} was similar to that for {Ln₂Te₂W₃₄}, and the only difference is that the pH of the reaction mixture was adjusted to 1.9. When the rod-shaped crystals were obtained, the pH of the mother liquor is 2.9. Element analysis (%) for {DyTeW₁₇}: calcd. C 3.20, N 1.87, Na

0.88, W 59.6, Te 2.43, Dy 3.10; found: C 3.23, N 1.78, Na 0.96, W 60.6, Te 2.40, Dy 3.06; yield: 17% based on W. Element analysis (%) for {HoTeW₁₇}: calcd. C 3.16, N 1.84, Na 0.86, W 58.7, Te 2.40, Ho 3.10; found: C 3.20, N 1.73, Na 0.86, W 57.2, Te 2.34, Ho 3.09; yield: 17% based on W. Element analysis (%) for {ErTeW₁₇}: calcd. C 3.21, N 1.87, Na 0.88, W 59.7, Te 2.44, Er 3.20; found: C 3.21, N 1.73, Na 0.89, W 60.8, Te 2.50, Er 3.15; yield: 20% based on W. Element analysis (%) for {TmTeW₁₇}: calcd. C 3.22, N 1.88, Na 0.88, W 59.9, Te 2.45, Tm 3.24; found: C 3.23, N 1.75, Na 0.87, W 58.9, Te 2.50, Tm 3.20; yield: 20% based on W. Element analysis (%) for {YbTeW₁₇}: C 3.16, N 1.85, Na 0.87, W 58.8, Te 2.40, Yb 3.26; found: C 3.32, N 1.78, Na 0.83, W 58.2, Te 2.40, Yb 3.26; yield: 19% based on W. Element analysis (%) for {LuTeW₁₇}: C 3.15, N 1.84, Na 0.86, W 58.6, Te 2.39, Lu 3.28; found: C 3.09, N 1.80, Na 0.86, W 59.5, Te 2.46, Lu 3.35; yield: 20% based on W.

Synthesis of (DMAH)_n{H_{3-n}Ln(H₂O)₄[TeW₆O₂₄]}⁻ mH₂O: ({LnTeW₆}, Ln = Dy³⁺, *n* = 1, *m* = 4; Ho³⁺, *n* = 2, *m* = 1; Er³⁺, *n* = 1, *m* = 10; Tm³⁺, *n* = 2, *m* = 8; Yb³⁺, *n* = 1, *m* = 7.5; Lu³⁺, *n* = 1.5, *m* = 10).

{LnTeW₆} was synthesized by the procedure similar to that for {Ln₂Te₂W₃₄} except that pH = 2.3. The hexagon-shaped crystals were observed after 1 month, and at that time the pH of the mother liquor is 3.2. Element analysis (%) for {DyTeW₆}: calcd. C 1.22, N 0.71, W 56.0, Te 6.48, Dy 8.25; found: C 1.14, N 0.68, W 55.7, Te 6.45, Dy 8.21; yield: 13% based on W. Element analysis (%) for {HoTeW₆}: calcd. C 2.49, N 1.45, W 57.1, Te 6.61, Ho 8.54; found: C 2.56, N 1.43, W 57.5, Te 6.67, Ho 8.59; yield: 16% based on W. Element analysis (%) for {ErTeW₆}: calcd. C 1.15, N 0.67, W 53.0, Te 6.13, Er 8.03; found: C 1.10, N 0.65, W 53.6, Te 6.18, Er 8.10; yield: 16% based on W. Element analysis (%) for {TmTeW₆}: calcd. C 2.30, N 1.34, W 52.7, Te 6.10, Tm 8.07; found: C 2.24, N 1.25, W 52.5, Te 6.06, Tm 8.01; yield: 17% based on W. Element analysis (%) for {YbTeW₆}: calcd. C 1.18, N 0.69, W 54.0, Te 6.25, Yb 8.47; found: C 1.14, N 0.75, W 54.2, Te 6.28, Yb 8.51; yield: 18% based on W. Element analysis (%) for {LuTeW₆}: calcd. C 1.71, N 0.99, W 52.2, Te 6.04, Lu 8.28; found: C 1.74, N 1.03, W 51.8, Te 6.01, Lu 8.23; yield: 20% based on W.

Catalytic Tests

Before the catalytic reaction, ground crystal samples were pretreated in a vacuum oven at 100°C for 3 h. The scanning electron microscopy (SEM) image (**Supplementary Figure 9**) shows that, after the pretreatment, micron-sized samples with an irregular morphology were obtained. Typically, aldehyde or ketone (1 mmol), trimethylsilylcyanide (TMSCN, 2 mmol), and catalysts (2 mol%) were loaded into a 25 ml Shrek tube, which was purged three times with argon gas and heated at 45°C for 12 h. After the reaction, the mixture was diluted with 2 ml acetonitrile and added with naphthalene (0.75 mmol) as internal standard. Finally, the mixture was centrifuged and monitored quantitatively by gas chromatography. The catalysts were collected, washed with acetonitrile, and dried under vacuum for the characterization and the next run.

RESULTS AND DISCUSSIONS

Syntheses and Structures

All crystal compounds were prepared by using $\text{Na}_2\text{WO}_4 \cdot 2\text{H}_2\text{O}$, $\text{Te}(\text{OH})_6$, dimethylamine hydrochloride, citric acid, and $\text{LnCl}_3 \cdot 6\text{H}_2\text{O}$ as starting materials in aqueous solution. Although citric acid does not appear in the final structures, the control experiments show that citric acid is important during the synthetic process. When we used another weak organic acid (e.g., acetic acid or amino acid) instead of citric acid, the yields of these crystal compounds dramatically decreased. According to previous investigations, we speculate that citric acid might play the role of a protective agent to coordinate with Ln^{3+} ions in preventing the formation of precipitates (Li et al., 2012; Wang et al., 2015). Moreover, it was found that dimethylamine hydrochloride is indispensable for the synthesis of crystal compounds. In the absence of dimethylamine hydrochloride, under the same reaction conditions, only numerous precipitation was obtained.

Description of $\{\text{Ln}_2\text{Te}_2\text{W}_{34}\}$ and $\{\text{LnTeW}_{17}\}$ Structures

Single-crystal X-ray crystallographic analyses reveal that both $\{\text{Ln}_2\text{Te}_2\text{W}_{34}\}$ and $\{\text{LnTeW}_{17}\}$ crystallize in the triclinic space group of *P-1*. $\{\text{LnTeW}_{17}\}$ is mono- Ln^{3+} -substituted Dawson-like POMs, while $\{\text{Ln}_2\text{Te}_2\text{W}_{34}\}$ has 2:2 dimeric clusters based on $\{\text{LnTeW}_{17}\}$ ($\text{Ln} = \text{Dy}^{3+}, \text{Ho}^{3+}, \text{Er}^{3+}, \text{Tm}^{3+}, \text{Yb}^{3+}, \text{Lu}^{3+}$). Due to the structural similarity, only the structures of $\{\text{Dy}_2\text{Te}_2\text{W}_{34}\}$ and $\{\text{DyTeW}_{17}\}$ are described here. $\{\text{DyTeW}_{17}\}$ consists of one Dy^{3+} ion, one $\{\text{TeW}_{17}\text{O}_{61}\}$ polyanion, seven DMAH^+ cations, two Na^+ ions, two protons, and four coordinated and 23 lattice water molecules. Dawson-like $\{\text{TeW}_{18}\text{O}_{62}\}$ was first reported by Cronin and Long in 2009 (Yan et al., 2009), where a $\{\text{Te}^{\text{VI}}\text{O}_6\}$ octahedron is encapsulated into $\{\text{W}_{18}\text{O}_{54}\}$ cage (Figure 1A). The $\{\text{TeW}_{17}\text{O}_{61}\}$ can be regarded as a monovacant structure of $\{\text{TeW}_{18}\text{O}_{62}\}$ formed by losing one $[\text{WO}]^{4+}$ from the belt position. Compared with $\{\text{TeW}_{18}\text{O}_{62}\}$, the $\{\text{Te}^{\text{VI}}\text{O}_6\}$ octahedron in $\{\text{DyTeW}_{17}\}$ still lies in the center of the cluster but exhibits a slight distortion because one $[\text{WO}]^{4+}$ unit is replaced by a Dy^{3+} ion. The Te-O bond lengths of $\{\text{DyTeW}_{17}\}$ are in the range of 1.930(5)–2.010(6) Å, deviating from an ideal bond length [1.981(6) Å] in $\{\text{TeW}_{18}\text{O}_{62}\}$. The Dy^{3+} ion is incorporated into the vacant position of $\{\text{TeW}_{17}\text{O}_{61}\}$ (Figure 1B) and coordinated with eight oxygen atoms: four from monovacant POM and four from coordinated water molecules. The inserted Dy^{3+} ion exhibits a distorted bicapped trigonal prismatic geometry with Dy-O bond lengths of 2.292(6)–2.464(7) Å (Supplementary Figure 1C). Due to the contraction effect of lanthanide, the Ln-O bond lengths decrease with the decrease of Ln^{3+} ionic radii (shown in Supplementary Table 2).

$\{\text{Dy}_2\text{Te}_2\text{W}_{34}\}$ is composed of two Dy^{3+} ions, two monovacant $[\text{TeW}_{17}\text{O}_{61}]^{14-}$ polyanions, 16 DMAH^+ cations, six protons, and six coordinated and 23 lattice H_2O molecules. The dimeric $\{\text{Dy}_2\text{Te}_2\text{W}_{34}\}$ is composed of two mono-substituted $\{\text{DyTeW}_{17}\}$ subunits, which are connected by a belt-to-belt linking mode through Dy-O bonds (Figure 1C). In this cluster, the two Dy^{3+} ions also display distorted bicapped

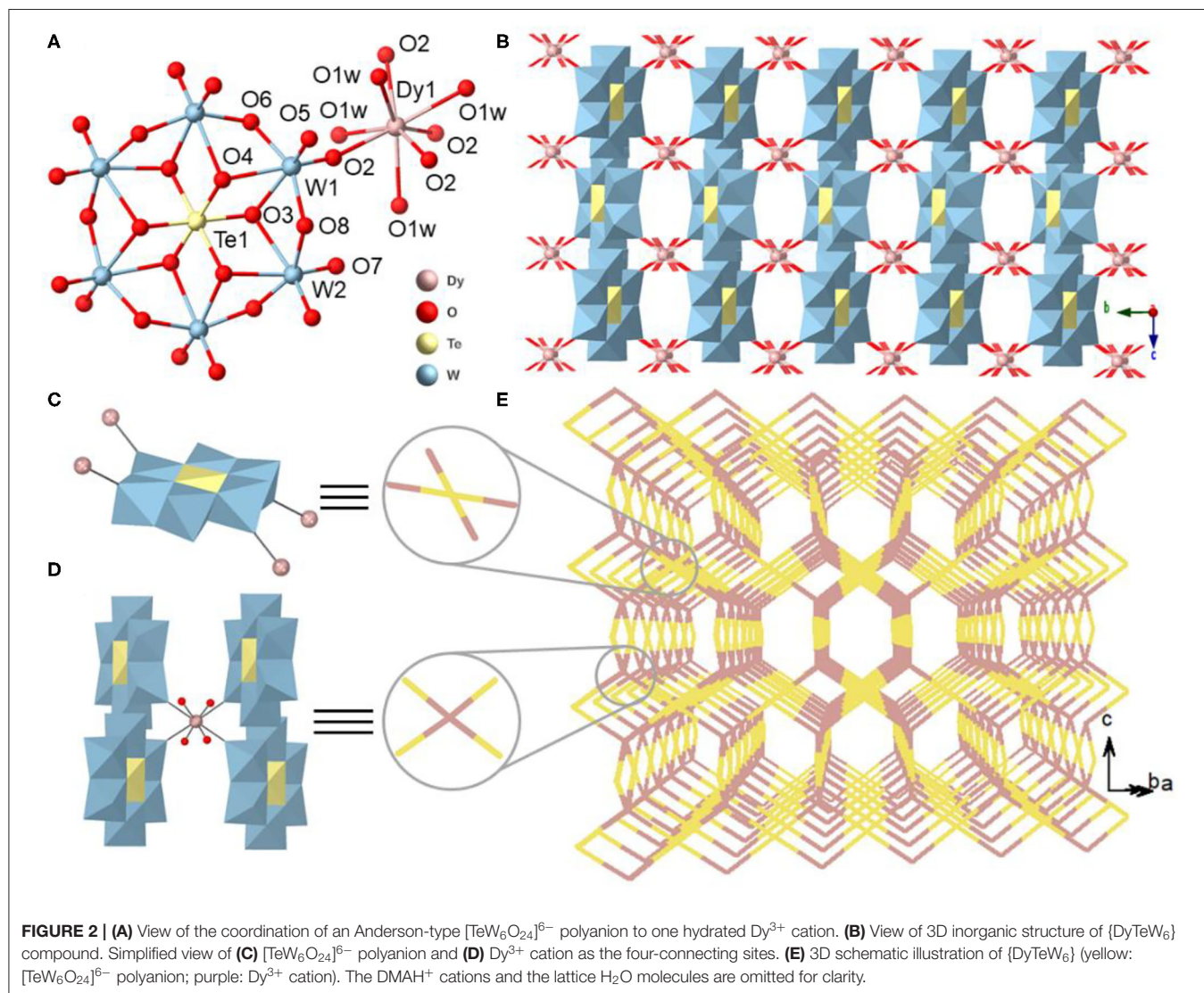
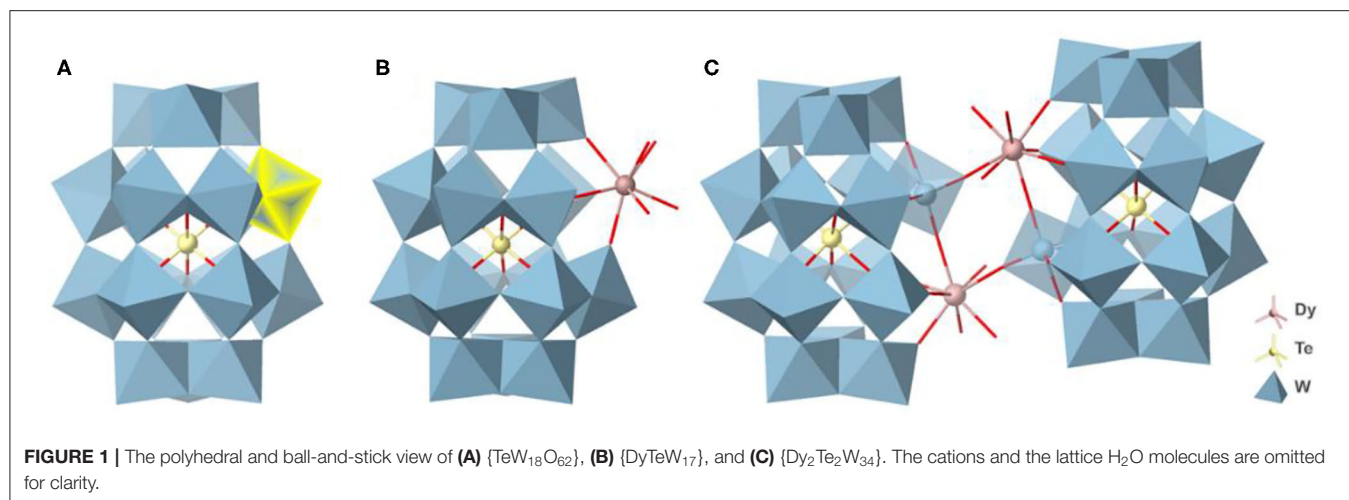
trigonal prismatic coordination geometries, coordinating by five terminal oxygen atoms (O4, O5, O6, O7, and O8) from two monovacant $[\text{TeW}_{17}\text{O}_{61}]^{14-}$ polyanions [Dy-O: 2.305(6)–2.374(7) Å] and three H_2O molecules [O1w, O2w and O3w) (Dy-O: 2.370(8)–2.434(9) Å] (Supplementary Figure 1E).

Description of $\{\text{LnTeW}_6\}$ Structures

Single-crystal X-ray crystallographic analyses reveal that the six $\{\text{LnTeW}_6\}$ compounds are isostructural and crystallize in the orthorhombic space group of *Cccm*. As a result, only the structure of $\{\text{DyTeW}_6\}$ is described in detail. $\{\text{DyTeW}_6\}$ contains one Dy^{3+} ion, one $[\text{TeW}_6\text{O}_{24}]^{6-}$ polyanion, one DMAH^+ cation, two protons, and four coordinated and four lattice H_2O molecules. The $[\text{TeW}_6\text{O}_{24}]^{6-}$ cluster shows an A-type Anderson structure where the central Te(VI) is surrounded by six edge-sharing WO_6 octahedra (Figure 2A). The octahedral $\{\text{TeO}_6\}$ has a slight distortion with O-Te-O bond angles in the range of 85.0(2)° to 95.0(2)°.

As shown in Figure 2C, each $[\text{TeW}_6\text{O}_{24}]^{6-}$ acts as a four-connecting node and connects with four Dy^{3+} ions through the terminal O2 atoms. The Dy^{3+} center exhibits a square antiprismatic geometry completed by four H_2O molecules (O1w) and four terminal oxygen atoms (O2) from four adjacent $[\text{TeW}_6\text{O}_{24}]^{6-}$ polyanions, and the Dy-O bond lengths are from 2.410(4) to 2.342(4) Å (Supplementary Figure 2A). As shown in Figure 2B and Supplementary Figure 2B, the alternating connection of $[\text{TeW}_6\text{O}_{24}]^{6-}$ polyanions and Dy^{3+} cations by sharing O2 atoms leads to a 3D inorganic framework. From the topological views, both $[\text{TeW}_6\text{O}_{24}]^{6-}$ and Dy^{3+} can be regarded as four-connecting sites (Figures 2C,D) and a (4,4)-connected PtS topology can be abstracted (Figure 2E).

It was found that the assembly of three types of Ln-containing tungstotellurates(VI) is pH dependent. Using $\{\text{TeW}_{17}\text{O}_{61}\}$ as a building block, dimeric $\{\text{Ln}_2\text{Te}_2\text{W}_{34}\}$ and mono-substituted $\{\text{LnTeW}_{17}\}$ were isolated at pH 1.7 and 1.9, respectively. At pH 1.8, $\{\text{Ln}_2\text{Te}_2\text{W}_{34}\}$ and $\{\text{LnTeW}_{17}\}$ crystallized together. When the solution pH was adjusted to 2.3, 3D inorganic frameworks $\{\text{LnTeW}_6\}$ based on Anderson-type $[\text{TeW}_6\text{O}_{24}]^{6-}$ were obtained. The results indicate that the size of tungstotellurates clusters decreases with the increase of pH. A similar trend is reported in Tb-containing tungstotellurates(VI) (Shang et al., 2018). In addition, we found that the assembly of Ln-containing POMs is influenced by the type of Ln^{3+} ions. The use of Ln^{3+} ions with a relatively smaller ionic radius [e.g., Tb^{3+} (Shang et al., 2018), Dy^{3+} , Ho^{3+} , Er^{3+} , Tm^{3+} , Yb^{3+} , or Lu^{3+}] leads to the formation of $\{\text{Ln}_2\text{Te}_2\text{W}_{34}\}$, $\{\text{LnTeW}_{17}\}$, and $\{\text{LnTeW}_6\}$ in the pH range of 1.7–2.3. However, when starting from Ln^{3+} ions with a relatively larger ionic radius (e.g., La^{3+} , Ce^{3+} , Pr^{3+} , Nd^{3+} , Sm^{3+} , or Eu^{3+}), under the otherwise identical conditions only precipitate or $\{\text{TeW}_{18}\text{O}_{62}\}$ clusters were observed. Notably, dimeric clusters, $[\text{H}_{10}(\text{WO}_2)\{\text{Ln}(\text{H}_2\text{O})_5(\text{TeW}_{18}\text{O}_{65})_2\}]^{12-}$, were prepared at pH 1.5 by using La^{3+} , Ce^{3+} , Pr^{3+} , Nd^{3+} , Sm^{3+} , Eu^{3+} , or Tb^{3+} , where two $\{\text{TeW}_{18}\text{O}_{65}\}$ units are bridged by one $\{\text{WO}_2\}$ and two Ln^{3+} (Shang et al., 2018; Yang et al., 2018). Nevertheless, such structural motif cannot be obtained when using Dy^{3+} , Ho^{3+} , Er^{3+} , Tm^{3+} , Yb^{3+} , or Lu^{3+} as starting materials. Therefore,

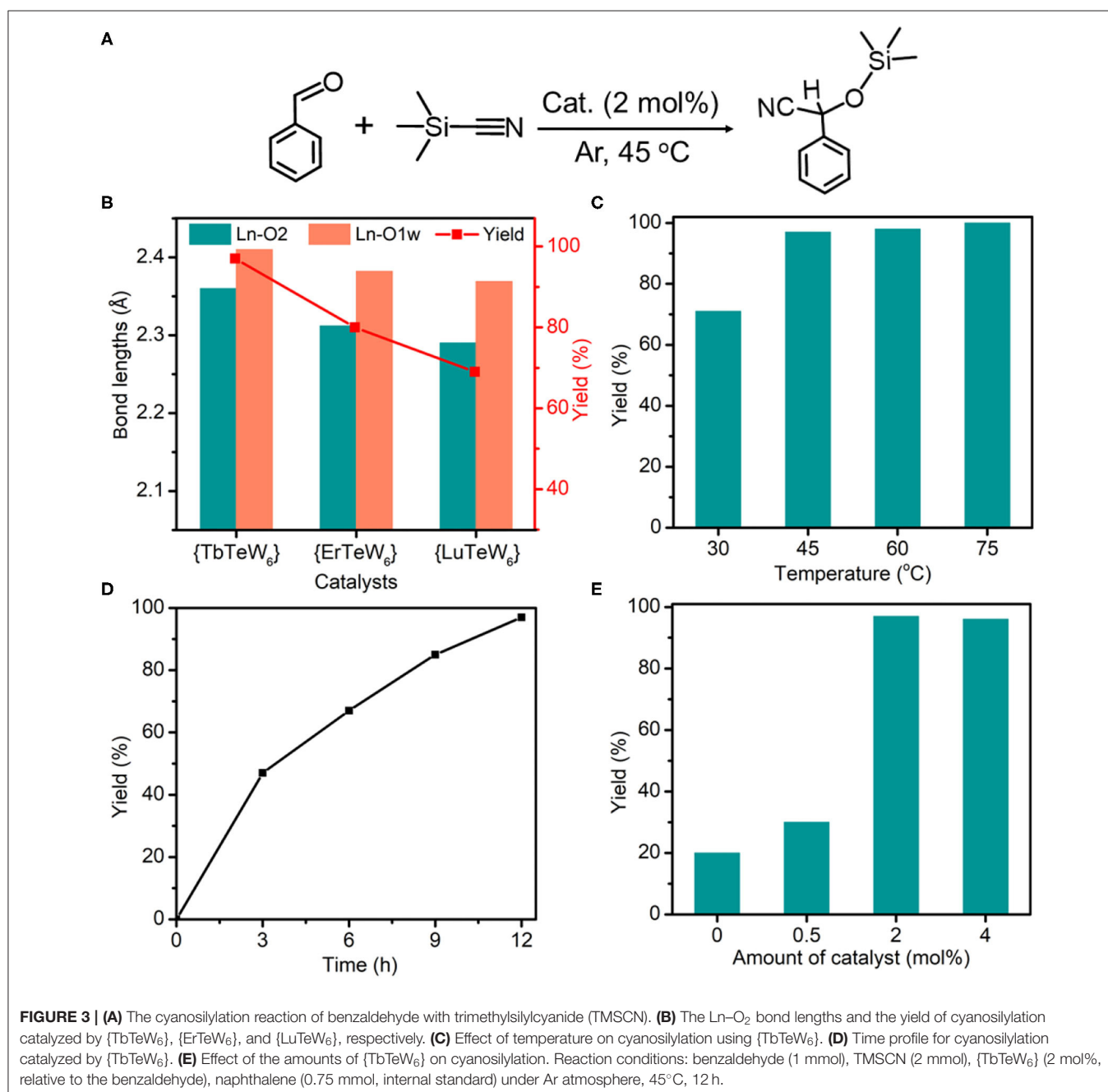


it is obvious that both pH and the type of Ln^{3+} ions have a significant impact on the assembly of these Ln-containing tungstotellurates(VI) (Scheme 1).

FT-IR Spectra

Since both $\{\text{Ln}_2\text{Te}_2\text{W}_{34}\}$ and $\{\text{LnTeW}_{17}\}$ are based on monovacant $\{\text{TeW}_{17}\text{O}_{61}\}$, their FT-IR spectra exhibit similar characteristic absorption peaks. As shown in **Supplementary Figures 3, 4**, the characteristic peaks at $1,020\text{ cm}^{-1}$ correspond to the antisymmetric stretching vibrations of Te-O bonds and the peaks at $942\text{--}948$, $812\text{--}818$, and $743\text{--}757\text{ cm}^{-1}$ are attributed to the vibrations of terminal $\text{W}=\text{O}$ bonds,

bridging $\text{W}-\text{O}_b-\text{W}$ (b: edge-shared O atoms) and $\text{W}-\text{O}_c-\text{W}$ (c: corner-shared O atoms), respectively. Compared with the plenary Dawson-like $[\text{TeW}_{18}\text{O}_{62}]^{10-}$ ($1,019$, 949 , and 799 cm^{-1}) (Yan et al., 2009), some characteristic absorption peaks of POMs are slightly shifted, which might be caused by inserting Ln^{3+} ions in the vacant site of monovacant $\{\text{TeW}_{17}\text{O}_{61}\}$. The FT-IR spectra of $\{\text{LnTeW}_6\}$ are illustrated in **Supplementary Figure 5**. The characteristic peaks in the range of $1,000\text{--}400\text{ cm}^{-1}$ are very similar. The peaks between 970 and 950 cm^{-1} are assigned to the terminal $\text{W}=\text{O}$ bonds, and those in the range of $920\text{--}630\text{ cm}^{-1}$ are the characteristic stretching vibrations of the $\text{W}-\text{O}-\text{W}$ bridges.



Moreover, the characteristic peaks of DMAH⁺ counteranions can be observed in these compounds. The peaks at 3,110–3,132 and 2,778–2,790 cm⁻¹ are assigned to the stretching vibrations of N-H and C-H bonds, respectively, while the peaks at 1,558–1,640 and 1,456–1,466 cm⁻¹ are attributed to the bending vibrations of N-H and C-H bonds, respectively. The broad peaks at 3,400–3,432 cm⁻¹ are the stretching vibrations of H₂O molecules. In addition, we observed that the crystals of Ln-containing tungstotellurates(VI) can easily turn to powder when leaving the mother liquor due to the loss of lattice water molecules. However, the POM skeleton is still maintained, which has been demonstrated by the FT-IR spectra.

Catalytic Activities of {LnTeW₆}

Our previous electrospray ionization–mass spectrometry investigations show that the {Tb₂Te₂W₃₄} and {TbTeW₁₇} clusters are unstable in solution, dissociating into stable {TeW₁₈O₆₂} and other fragments (Shang et al., 2018). In comparison, the 3D inorganic framework {LnTeW₆} is stable, and the Lewis acidic centers (Ln³⁺) are accessible after removing the lattice and the coordinated water molecules. The cyanosilylation reaction is an important method to prepare cyanohydrins, which can be further converted into value-added chemicals (e.g., α -hydroxy ketones, α -hydroxy acids, and β -amino alcohols) and drug molecules (Brunel and Holmes, 2004; Jia et al., 2014). Therefore, the cyanosilylation of benzaldehyde with TMSCN under solvent-free conditions was used as a reaction model to evaluate the Lewis acid catalytic activity of {LnTeW₆} (Figure 3A). As no byproduct was obtained in the reaction, the yield of cyanohydrin trimethylsilyl ethers was calculated based on the conversion of benzaldehyde.

In our work, seven isostructural {LnTeW₆} frameworks (Ln = Tb³⁺, Dy³⁺, Ho³⁺, Er³⁺, Tm³⁺, Yb³⁺, and Lu³⁺) were synthesized, which provides a good platform to investigate the effect of Ln ionic radius on the Lewis acid catalytic activity. As the decrease of ionic radius from Tb³⁺ (0.0923 Å) to Lu³⁺ (0.0848 Å) is unobvious, only three representative catalysts, {TbTeW₆}, {ErTeW₆}, and {LuTeW₆}, were used. As shown

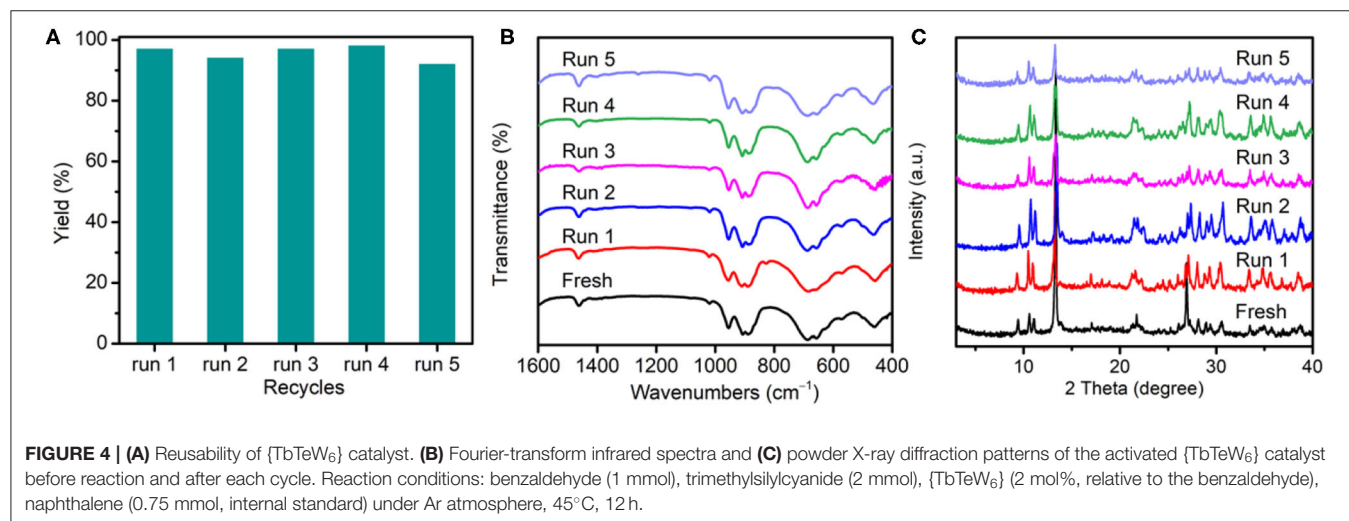
in Figure 3B, all of {TbTeW₆}, {ErTeW₆}, and {LuTeW₆} can promote the cyanosilylation reaction with a yield of 69–97%. In contrast, only 20% yield was obtained in the absence of a catalyst. Interestingly, it was found that the catalytic activity of {LnTeW₆} decreased with the decrease of Ln ionic radius, giving the order of {TbTeW₆} (97%) > {ErTeW₆} (80%) > {LuTeW₆} (69%). On the one hand, the Ln-O2 bond lengths (O2: terminal oxygen atom of {TeW₆O₂₄}) decrease from Tb³⁺ to Lu³⁺ in the order of Tb-O2 (2.360 Å) > Er-O2 (2.312 Å) > Lu-O2 (2.290 Å). The decrease of Ln-O2 bond length leads to the increase of steric hindrance around Ln³⁺ ions, and as a result, it becomes difficult for the substrates to access the Lewis acidic centers. On the other hand, the Ln-O1w bond lengths (O1w: the coordinated H₂O molecules) also decreases from Tb³⁺ to Lu³⁺ (Tb-O1w: 2.410 Å, Er-O1w: 2.382 Å, and Lu-O1w: 2.369 Å), making the removal of coordinated H₂O molecules difficult and resulting in the catalytic activity of Ln³⁺ ions being reduced. With the good performance of {TbTeW₆}, it is used in the following experiments.

To explore the optimal reaction conditions, the influences of reaction temperature, time, and amount of catalyst on the cyanosilylation reaction were systematically investigated.

TABLE 1 | The cyanosilylation reaction catalyzed by {TbTeW₆}^a.

		
1 (97%)	2 (100%)	3 (49%)
		
4 (66%)	5 (29%)	6 (8%)

^aReaction conditions: substrate (1 mmol), trimethylsilylcyanide (2 mmol), {TbTeW₆} (2 mol%, relative to the benzaldehyde), naphthalene (0.75 mmol, internal standard) under Ar atmosphere, 45°C, 12 h. The yield of the corresponding cyanohydrin trimethylsilyl ethers was monitored by gas chromatography with flame ionization detector.



As shown in **Figure 3C**, the reaction was conducted in the temperature range of 30–75°C, and a satisfactory yield (97%) was achieved at 45°C. The yield of 2-phenyl-2-[(trimethylsilyloxy)acetonitrile increases with the reaction time, and the maximum yield was reached after 12 h at 45°C (**Figure 3D**). As shown in **Figure 3E**, the catalyst amount of 2 mol% (relative to benzaldehyde) is an optimized dosage for this reaction.

To verify the heterogeneity of {TbTeW₆}, the catalyst was incubated in solvent at 45°C for 12 h, and the inductively coupled plasma result reveals that a negligible amount of Te, Tb, and W was detected in the filtrate. Moreover, the reusability and the stability of {TbTeW₆} was tested under the optimized conditions. As shown in **Figure 4A**, {TbTeW₆} could be reused for five times without a significant loss of its catalytic activity. The FT-IR spectra and powder X-ray diffraction (PXRD) patterns of the {TbTeW₆} used were basically identical to those of the fresh ones (**Figures 4B,C**), suggesting that the structure of {TbTeW₆} was maintained after five cycles and that Lewis acidic center Tb³⁺ is successfully stabilized by {TeW₆O₂₄} clusters. The SEM images show that the ground {TbTeW₆} has an irregular morphology in micrometers before the reaction and after five recycles (**Supplementary Figure 9**). In addition, Na₆TeW₆O₂₄ and TbCl₃ · 6H₂O were used in the reaction and gave a yield of 100%. However, Na₆TeW₆O₂₄ is unstable under the turnover conditions, as confirmed by FT-IR and PXRD characterization (**Supplementary Figure 10**), and TbCl₃ · 6H₂O cannot be reused.

The effect of substituents on aromatic aldehydes was investigated, and the results are shown in **Table 1**. Aromatic aldehyde with electron-withdrawing group (chloro) is beneficial to the cyanosilylation reaction, giving a yield of up to 100% (2 in **Table 1**). However, a significant decrease of yield was observed by using aromatic aldehydes with electron-donating groups (methoxy) (3–5 in **Table 1**). Among them, the yield of **5** (29%) with two methoxy substituents is much lower than those of **3** (49%) and **4** (66%) with one methoxy substituent. Generally, ketones are less reactive than aldehydes in cyanosilylation reaction, and thus only 8% yield was obtained using acetophenone as substrate (6 in **Table 1**).

CONCLUSIONS

In summary, a series of Ln-containing tungstotellurates(VI) have been isolated and structurally characterized. The assembly of

dimeric {Ln₂Te₂W₃₄}, mono-substituted {LnTeW₁₇}, and 3D inorganic framework {LnTeW₆} is pH dependent, which were formed at pH 1.7, 1.9, and 2.3, respectively. Importantly, the type of Ln³⁺ ions plays an important role in the assembly process. The three types of Ln-containing POMs can be synthesized by using Tb³⁺-Lu³⁺ ions with a relatively smaller radius, while when starting from La³⁺-Eu³⁺ ions only precipitation or {TeW₁₈O₆₂} clusters were observed. Moreover, three {LnTeW₆} (Ln = Tb³⁺, Er³⁺, Lu³⁺) are selected as heterogeneous Lewis acid catalysts for the cyanosilylation reaction. It was found that the catalytic activity of {LnTeW₆} decreases with the decrease of Ln³⁺ ionic radius. The {TbTeW₆} catalyst exhibits excellent stability and can be reused for five times without a significant loss of activity. The successful isolation of Ln-containing POMs not only contributes to the understanding of Ln-containing POM assembly but also provides a good platform to investigate the influence of Ln ionic radius on their Lewis acid catalytic activity.

DATA AVAILABILITY STATEMENT

The datasets presented in this study can be found in online repositories. The names of the repository/repositories and accession number(s) can be found in the article/**Supplementary Material**.

AUTHOR CONTRIBUTIONS

YC and CH supervised the project. JL, SS, and NZ prepared the catalysts. ZLin and ZY analyzed the crystallographic data. JL performed the catalytic experiments and wrote the manuscript. ZLi participated in the analysis of the results. All authors contributed to the article and approved the submitted version.

FUNDING

This work was financially supported by the National Natural Science Foundation of China (21671019, 21871026, 21771020, and 21971010).

SUPPLEMENTARY MATERIAL

The Supplementary Material for this article can be found online at: <https://www.frontiersin.org/articles/10.3389/fchem.2020.598961/full#supplementary-material>

REFERENCES

- Arab Fashapoyeh, M., Mirzaei, M., Eshtiagh-Hosseini, H., Rajagopal, A., Lechner, M., Liu, R., et al. (2018). Photochemical and electrochemical hydrogen evolution reactivity of lanthanide-functionalized polyoxotungstates. *Chem. Commun.* 54, 10427–10430. doi: 10.1039/C8CC06334F
- Boglio, C., Lemièrre, G., Hasenknopf, B., Thorimbert, S., Lacôte, E., and Malacria, M. (2006). Lanthanide complexes of the monovacant dawson polyoxotungstate [α₁-P₂W₁₇O₆₁]¹⁰⁻ as selective and recoverable lewis acid catalysts. *Angew. Chem. Int. Ed.* 45, 3324–3327. doi: 10.1002/anie.200600364
- Brunel, J. M., and Holmes, I. P. (2004). Chemically catalyzed asymmetric cyanohydrin syntheses. *Angew. Chem. Int. Ed.* 43, 2752–2778. doi: 10.1002/anie.200300604
- Chen, W. C., Jiao, C. Q., Wang, X. L., Shao, K. Z., and Su, Z. M. (2019). Self-assembly of nanoscale lanthanoid-containing selenotungstates: synthesis, structures, and magnetic studies. *Inorg. Chem.* 58, 12895–12904. doi: 10.1021/acs.inorgchem.9b01830
- Chen, W. C., Li, H. L., Wang, X. L., Shao, K. Z., Su, Z. M., and Wang, E. B. (2013). Assembly of cerium(III)-stabilized polyoxotungstate nanoclusters with SeO₃²⁻/TeO₃²⁻ templates: from single polyoxoanions to

- inorganic hollow spheres in dilute solution. *Chem. Eur. J.* 19, 11007–11015. doi: 10.1002/chem.201300615
- Chen, W. C., Qin, C., Wang, X. L., Li, Y. G., Zang, H. Y., Shao, K. Z., et al. (2015). Assembly of a large cerium(III)-containing tungstotellurites(IV) nanocluster: $[\text{Ce}_{10}\text{Te}_8\text{W}_{88}\text{O}_{298}(\text{OH})_{12}(\text{H}_2\text{O})_{40}]^{18-}$. *Dalton Trans.* 44, 11290–11293. doi: 10.1039/C5DT01711D
- Chen, W. C., Wang, X. L., Jiao, Y. Q., Huang, P., Zhou, E. L., Su, Z. M., et al. (2014). pH-controlled and sulfite anion-directed assembly of a family of cerium(III)-containing polyoxotungstates clusters. *Inorg. Chem.* 53, 9486–9497. doi: 10.1021/ic500442k
- Chen, Y., Sun, L., Chang, S., Chen, L., and Zhao, J. (2018). Synergistic effect between different coordination geometries of lanthanides and various coordination modes of 2-picolinic acid ligands tuning three types of rare 3d-4f heterometallic tungstotellurates. *Inorg. Chem.* 57, 15079–15092. doi: 10.1021/acs.inorgchem.8b02103
- Clemente-Juan, J. M., Coronado, E., and Gaita-Ariño, A. (2012). Magnetic polyoxometalates: from molecular magnetism to molecular spintronics and quantum computing. *Chem. Soc. Rev.* 41, 7464–7478. doi: 10.1039/c2cs35205b
- Cronin, L., and Müller, A. (2012). From serendipity to design of polyoxometalates at the nanoscale, aesthetic beauty and applications. *Chem. Soc. Rev.* 41, 7333–7334. doi: 10.1039/c2cs90087d
- Dolomanov, O. V., Bourhis, L. J., Gildea, R. J., Howard, J. A. K., and Puschmann, H. (2009). OLEX2: a complete structure solution, refinement and analysis program. *J. Appl. Cryst.* 42, 339–341. doi: 10.1107/S0021889808042726
- Gao, J., Yan, J., Mitchell, S. G., Miras, H. N., Boulay, A. G., Long, D. L., et al. (2011). Self-assembly of a family of macrocyclic polyoxotungstates with emergent material properties. *Chem. Sci.* 2, 1502–1508. doi: 10.1039/c1sc00150g
- Granadeiro, C. M., Ferreira, R. A. S., Soares-Santos, P. C. R., Carlos, L. D., Trindade, T., and Nogueira, H. I. S. (2010). Lanthanopolyoxotungstates in silica nanoparticles: multi-wavelength photoluminescent core/shell materials. *J. Mater. Chem.* 20, 3313–3318. doi: 10.1039/b919691a
- Han, Q., Liu, J. C., Wen, Y., Chen, L. J., Zhao, J. W., and Yang, G. Y. (2017a). Telluritungstate-based organotin-rare-earth heterometallic hybrids with four organic components. *Inorg. Chem.* 56, 7257–7269. doi: 10.1021/acs.inorgchem.7b00924
- Han, Q., Wen, Y., Liu, J. C., Zhang, W., Chen, L. J., and Zhao, J. W. (2017b). Rare-earth-incorporated telluritungstate hybrids functionalized by 2-picolinic acid ligands: syntheses, structures, and properties. *Inorg. Chem.* 56, 13228–13240. doi: 10.1021/acs.inorgchem.7b02009
- Hill, C. L. (1998). Introduction: polyoxometalates/multicomponent molecular vehicles to probe fundamental issues and practical problems. *Chem. Rev.* 98, 1–2. doi: 10.1021/cr960395y
- Ismail, A. H., Nsouli, N. H., Dickman, M. H., Knez, J., and Kortz, U. (2009). The 20-Tungsto-4-tellurate(IV) $[\text{H}_2\text{Te}_4\text{W}_{20}\text{O}_{80}]^{22-}$ and the 15-tungstotellurate(IV) $[\text{NaTeW}_{15}\text{O}_{54}]^{13-}$. *J. Cluster Sci.* 20, 453–465. doi: 10.1007/s10876-009-0245-6
- Jia, Y., Zhao, S., and Song, Y. F. (2014). The application of spontaneous flocculation for the preparation of lanthanide-containing polyoxometalates intercalated layered double hydroxides: highly efficient heterogeneous catalysts for cyanosilylation. *Appl. Catal. A Gen.* 487, 172–180. doi: 10.1016/j.apcata.2014.09.005
- Kaushik, R., Khan, I., Saini, M. K., Hussain, F., and Sadakane, M. (2018). Synthesis and characterization of carbonate-encapsulated ytterbium- and yttrium-containing polyoxotungstates. *Acta Crystallogr. Sect. C* 74, 1355–1361. doi: 10.1107/S2053229618011841
- Li, F., Guo, W., Xu, L., Ma, L., and Wang, Y. (2012). Two dysprosium-incorporated tungstoarsenates: synthesis, structures and magnetic properties. *Dalton Trans.* 41, 9220–9226. doi: 10.1039/c2dt12277d
- Li, S., Zhou, Y., Peng, Q., Wang, R., Feng, X., Liu, S., et al. (2018). Controllable synthesis and catalytic performance of nanocrystals of rare-earth-polyoxometalates. *Inorg. Chem.* 57, 6624–6631. doi: 10.1021/acs.inorgchem.8b00763
- Liu, J. C., Han, Q., Chen, L. J., Zhao, J. W., Streb, C., and Song, Y. F. (2018). Aggregation of giant cerium-bismuth tungstate clusters into a 3d porous framework with high proton conductivity. *Angew. Chem. Int. Ed.* 57, 8416–8420. doi: 10.1002/ange.201803649
- Liu, J. C., Zhao, J. W., and Song, Y. F. (2019). 1-D chain tungstotellurate hybrids constructed from organic-ligand-connecting iron-lanthanide heterometal encapsulated tetrameric polyoxotungstate units. *Inorg. Chem.* 58, 9706–9712. doi: 10.1021/acs.inorgchem.9b00618
- Liu, J. L., Jin, M. T., Chen, L. J., and Zhao, J. W. (2018). First dimethyltin-functionalized rare-earth incorporated telluritungstates consisting of $\{\text{B-}\alpha\text{-TeW}_7\text{O}_{28}\}$ and $\{\text{W}_5\text{O}_{18}\}$ mixed building units. *Inorg. Chem.* 57, 12509–12520. doi: 10.1021/acs.inorgchem.8b01486
- Ma, X., Yang, W., Chen, L., and Zhao, J. (2015). Significant developments in rare-earth-containing polyoxometalate chemistry: synthetic strategies, structural diversities and correlative properties. *CrystEngComm* 17, 8175–8197. doi: 10.1039/C5CE01240F
- Mialane, P., Lisnard, L., Mallard, A., Marrot, J., Antic-Fidancev, E., Aschehoug, P., et al. (2003). Solid-State and solution studies of $\{\text{Ln}_n(\text{SiW}_{11}\text{O}_{39})\}$ polyoxoanions: an example of building block condensation dependent on the nature of the rare earth. *Inorg. Chem.* 42, 2102–2108. doi: 10.1021/ic020486f
- Mougharbel, A. S., Bhattacharya, S., Bassil, B. S., Rubab, A., van Leusen, J., Kogerler, P., et al. (2020). Lanthanide-containing 22-tungsto-2-germanates $[\text{Ln}(\text{GeW}_{11}\text{O}_{39})_2]^{13-}$: synthesis, structure, and magnetic properties. *Inorg. Chem.* 59, 4340–4348. doi: 10.1021/acs.inorgchem.9b03271
- Ozeki, T., and Yamase, T. (1994). Effect of lanthanide contraction on the structures of the decatungstolanthanoate anions in $\text{K}_3\text{Na}_4\text{H}_2[\text{LnW}_{10}\text{O}_{36}]\cdot n\text{H}_2\text{O}$ (Ln = Pr, Nd, Sm, Gd, Tb, Dy) crystals. *Acta Crystallogr. Sect. B* 50:128. doi: 10.1107/S0108768193011553
- Ritchie, C., Alley, K. G., and Boskovic, C. (2010a). Lacunary tungstotellurates(IV): $[\text{Te}_2\text{W}_{17}\text{O}_{61}]^{12-}$, $[\text{Te}_2\text{W}_{16}\text{O}_{58}(\text{OH})_2]^{14-}$ and $[\text{Te}_2\text{W}_{18}\text{O}_{62}(\text{OH})_2]^{10-}$. *Dalton Trans.* 39, 8872–8874. doi: 10.1039/c0dt00547a
- Ritchie, C., Moore, E. G., Speldrich, M., Kogerler, P., and Boskovic, C. (2010b). Terbium polyoxometalate organic complexes: correlation of structure with luminescence properties. *Angew. Chem. Int. Ed.* 49, 7702–7705. doi: 10.1002/anie.201002320
- Schmidt, K. J., Schrobilgen, G. J., and Sawyer, J. F. (1986). Hexasodium hexatungstotellurate(VI) 22-hydrate. *Acta Crystallogr. Sect. C* 42, 1115–1118. doi: 10.1107/S0108270186093204
- Shah, H. S., Al-Oweini, R., Haider, A., Kortz, U., and Iqbal, J. (2014). Cytotoxicity and enzyme inhibition studies of polyoxometalates and their chitosan nanoassemblies. *Toxicol. Rep.* 1, 341–352. doi: 10.1016/j.toxrep.2014.06.001
- Shang, S., Lin, Z., Yin, A., Yang, S., Chi, Y., Wang, Y., et al. (2018). Self-assembly of Ln(III)-containing tungstotellurates(VI): correlation of structure and photoluminescence. *Inorg. Chem.* 57, 8831–8840. doi: 10.1021/acs.inorgchem.8b00693
- Sheldrick, G. M. (2015). Crystal structure refinement with SHELXL. *Acta Crystallogr. Sect. C* 71, 3–8. doi: 10.1107/S2053229614024218
- Suzuki, K., Sato, R., and Mizuno, N. (2013). Reversible switching of single-molecule magnet behaviors by transformation of dinuclear dysprosium cores in polyoxometalates. *Chem. Sci.* 4, 596–600. doi: 10.1039/C2S12619A
- Suzuki, K., Tang, F., Kikukawa, Y., Yamaguchi, K., and Mizuno, N. (2014). Visible-light-induced photoredox catalysis with a tetracerium-containing silicotungstate. *Angew. Chem. Int. Ed.* 53, 5356–5360. doi: 10.1002/anie.201403215
- Wang, Y., Sun, X., Li, S., Ma, P., Niu, J., and Wang, J. (2015). Generation of large polynuclear rare earth metal-containing organic-inorganic polytungstoarsenate aggregates. *Cryst. Growth Des.* 15, 2057–2063. doi: 10.1021/cg5012499
- Yan, J., Long, D. L., Wilson, E. F., and Cronin, L. (2009). Discovery of heteroatom-“embedded” $\text{Te}\{\text{W}_{18}\text{O}_{54}\}$ nanofunctional polyoxometalates by use of cryospray mass spectrometry. *Angew. Chem. Int. Ed.* 48, 4376–4380. doi: 10.1002/anie.200806343
- Yang, G. P., Shang, S. X., Yu, B., and Hu, C. W. (2018). Ce(III)-Containing tungstotellurate(vi) with a sandwich structure: an efficient Lewis acid-base catalyst for the condensation cyclization of 1,3-diketones with hydrazines/hydrazides or diamines. *Inorg. Chem. Front.* 5, 2472–2477. doi: 10.1039/C8QI00678D
- Zhang, D., Zhang, C., Chen, H., Ma, P., Wang, J., and Niu, J. (2012). Syntheses, structures and properties of dimeric rare earth derivatives based on monovacant keggins-type polyoxotungstates. *Inorg. Chim. Acta* 391, 218–223. doi: 10.1016/j.ica.2012.04.030

- Zhang, Y., Wang, D., Zeng, B., Chen, L., Zhao, J., and Yang, G. Y. (2020). An unprecedented polyhydroxycarboxylic acid ligand bridged multi-Eu^{III} incorporated tellurotungstate and its luminescence properties. *Dalton Trans.* 49, 8933–8948. doi: 10.1039/D0DT00729C
- Zhao, H. Y., Yang, B. F., and Yang, G. Y. (2017). Two new 2D organic–inorganic hybrids assembled by lanthanide-substituted polyoxotungstate dimers and copper–complex linkers. *Inorg. Chem. Commun.* 84, 212–216. doi: 10.1016/j.inoche.2017.08.027
- Zhao, J. W., Li, H. L., Ma, X., Xie, Z., Chen, L. J., and Zhu, Y. (2016a). Lanthanide-connecting and lone-electron-pair active trigonal-pyramidal-AsO₃ inducing nanosized poly(polyoxotungstate) aggregates and their anticancer activities. *Sci. Rep.* 6:26406. doi: 10.1038/srep26406
- Zhao, J. W., Li, Y. Z., Chen, L. J., and Yang, G. Y. (2016b). Research progress on polyoxometalate-based transition-metal-rare-earth heterometallic derived materials: synthetic strategies, structural overview and functional applications. *Chem. Commun.* 52, 4418–4445. doi: 10.1039/C5CC10447E
- Zhao, J. W., Li, Y. Z., Ji, F., Yuan, J., Chen, L. J., and Yang, G. Y. (2014). Syntheses, structures and electrochemical properties of a class of 1-D double chain polyoxotungstate hybrids [H₂dap][Cu(dap)₂]_{0.5}[Cu(dap)₂(H₂O)][Ln(H₂O)₃(α-GeW₁₁O₃₉)]·3H₂O. *Dalton Trans.* 43, 5694–5706. doi: 10.1039/C3DT53616E

Conflict of Interest: SS was employed by company China Resources Double-Crane Pharmaceutical Co., Ltd.

The remaining authors declare that the research was conducted in the absence of any commercial or financial relationships that could be construed as a potential conflict of interest.

Copyright © 2020 Li, Shang, Lin, Yao, Zhen, Li, Chi and Hu. This is an open-access article distributed under the terms of the Creative Commons Attribution License (CC BY). The use, distribution or reproduction in other forums is permitted, provided the original author(s) and the copyright owner(s) are credited and that the original publication in this journal is cited, in accordance with accepted academic practice. No use, distribution or reproduction is permitted which does not comply with these terms.